Inorg. Chem. **2005**, *44*, 8065–8075

Designing Molecular Bistability in Ruthenium Dimethyl Sulfoxide Complexes

Aaron A. Rachford,[†] Jeffrey L. Petersen,[‡] and Jeffrey J. Rack*[,†]

Department of Chemistry and Biochemistry, Ohio University, Athens, Ohio 45701, and C. Eugene Bennett Department of Chemistry, West Virginia University, Morgantown, West Virginia 26506-6045

Received May 14, 2005

Compounds of the type $[Ru(tpy)(L2)(dmso)]^{2+}$ (tpy is 2,2′:6′,2″-terpyridine; L2 can be 2,2′-bipyridine (bpy), *N,N,N′,N′*-tetramethylethylenediamine (tmen), 2-pyridine carboxylate (pic), acetylacetonate (acac), malonate (mal), or oxalate (ox)) have been studied by X-ray crystallography, electrochemistry, NMR, IR, and UV–vis spectroscopy. When L2 is bpy, tmen, or pic, the dmso ligand can be intramolecularly isomerized either electrochemically or photochemically. Isomerization is not observed when L2 is acac, mal, or ox. Isomerization results in a drastic change in the absorption spectrum, as well as in the voltammetry. Absorption maxima shift by 3470 (419–490 nm), 4775 (421–527 nm), and 4440 cm^{-1} (429–530 nm) for the bpy, pic, and tmen complexes, respectively. Reduction potentials for S-bonded and O-bonded complexes differ by 0.57, 0.75, and 0.62 V for the bpy, pic, and tmen complexes, respectively. Quantum yields of isomerization ($\phi_{S\rightarrow O}$) were determined for the bpy (0.024 ± 1), pic (0.25 ± 1), and tmen (0.007 ± 1) complexes. In comparison of these data to photosubstitution quantum yields, it appears that the isomerization mechanism does not involve the ligand field states. This result is surprising given the importance of these states in the photochemistry of ruthenium and osmium polypyridine complexes. These results and details of the mechanism are discussed.

Introduction

The development of photoswitchable bistable molecules is of interest due to potential use in applications such as optical molecular information storage, optical limiting devices, and molecular sensing.[1,2] For photonic devices, the design of such molecules requires the efficient conversion of light energy to potential energy. Photochromic compounds are a class of photonic devices which use light energy in bond-breaking and bond-making processes. Thus, bistable molecules are also of a fundamental interest in that the design of such molecules requires specific electronic structures in order to exhibit two stable interconvertible states.

Photoinduced or phototriggered linkage isomerizations have been observed in certain late transition metal complexes containing NO^+, NO_2^-, N_2, SO_2, and dmso (dimethyl sulfoxide).[3−5] For example, Ni(Cp)(NO) and $Na_2[M(CN)_5(NO)]$ ($M = Fe^{II}$, Ru^{II}, Os^{II}) feature both isonitrosyl (O-bonded) and η^2-NO (side-on) metastable bonding modes following irradiation of the N-bonded ground states at low temperatures.[6,7] Isonitrosyl coordination has been found in complexes in weak-field $[RuCl_5(NO)]^{2-}$, as well as porphyrin ligand environments [Fe(por)(NO)].[4,8] While dinitrogen isomerization in $[Ru(NH_3)_5]^{2+}$ fragments was initially investigated by Taube and Armor,[9,10] more recent crystallographic and vibrational studies have revealed the presence

* To whom correspondence should be addressed. E-mail: rack@helios.phy.ohiou.edu.
[†] Ohio University.
[‡] West Virginia University.

(1) Gutlich, P.; Garcia, Y.; Woike, T. *Coord. Chem. Rev.* **2001**, *219*, 839−879.
(2) Sato, O. *Acc. Chem. Res.* **2003**, *36*, 692−700.
(3) Fomitchev, D. V.; Novozhilova, I.; Coppens, P. *Tetrahedron* **2000**, *56*.
(4) Coppens, P.; Novozhilova, I.; Kovalevsky, A. *Chem. Rev.* **2002**, *102*, 861−883.
(5) Hortala, M. A.; Fabbrizzi, L.; Foti, F.; Licchelli, M.; Poggi, A.; Zema, M. *Inorg. Chem.* **2003**, *42*, 664−666.
(6) Fomitchev, D. V.; Furlani, T. R.; Coppens, P. *Inorg. Chem.* **1998**, *37*, 1519−1526.
(7) Carducci, M. D.; Pressprich, M. R.; Coppens, P. *J. Am. Chem. Soc.* **1997**, *119*, 2669−2678.
(8) Cheng, L.; Novozhilova, I.; Kim, C.; Kovalevsky, A.; Bagley, K. A.; Coppens, P.; Richter-Addo, G. B. *J. Am. Chem. Soc.* **2000**, *122*, 7142−7143.
(9) Armor, J. N.; Taube, H. *J. Am. Chem. Soc.* **1970**, *92*, 2560−2562.
(10) Pell, S.; Mann, R. H.; Taube, H.; Armor, J. N. *Inorg. Chem.* **1974**, *13*, 479−480.

10.1021/ic050778r CCC: $30.25
Published on Web 09/21/2005

of a metastable η^2-N_2 (side-on) binding in $[Os(NH_3)_5(N_2)]^{2+}$.[11] Expansion of these studies to include SO_2 has resulted in the identification of η^2-SO_2 binding mode in $[Ru(NH_3)_4(OH_2)(SO_2)]^{2+}$, which is formed from irradiation of the structurally characterized S-bonded ground state.[12] Investigations of dmso isomerizations of ruthenium complexes have shown that S-to-O isomerization may be induced electrochemically[13−17] or photochemically.[18−22] Despite these efforts, an encompassing mechanism which allows for the prediction of this reactivity has not emerged.

Our group has focused on dmso isomerization in ruthenium(II) polypyridine complexes.[19,20,22] The relatively intense visible charge-transfer transitions, well-established electrochemistry, and available synthetic procedures make this class of compounds particularly attractive. Furthermore, ruthenium polypyridine dmso complexes which undergo excited-state linkage isomerization also exhibit drastic changes in the absorption spectrum following irradiation. Concomitant with these absorption changes are dramatic shifts in the reduction potential. The combination of these features is desirable in the continued advancement of molecule-based devices.[23,24] Thus, the development of a methodology to understand and predict this reactivity is important from both a fundamental and applied perspective.

The focus of this study is $[Ru(tpy)(L2)(dmso)]^{z+}$ (tpy is 2,2′:6′,2″-terpyridine; L2 is a variable bidentate ligand) which features electrochemically and photochemically triggered isomerization of bound dmso. Certain bidentate ligands were chosen on the basis of their ability to modulate the Ru(III/II) reduction potential ($E^{\circ\prime}$). Variation of the bidentate ligand permits an examination of the kinetic and thermodynamic parameters of dmso isomerization. Our results show that strong field ligand environments promote excited state isomerization and that weak field ligand environments prohibit isomerization. The data also suggest that photoisomerization does not require intervention of ligand field states. This is a surprising result given the importance of these levels in ruthenium polypyridine photochemistry. Herein, we report the structural, electrochemical, and spectroscopic results on this family of complexes.

Experimental Section

Materials. The complexes $Ru(tpy)Cl_3$, [Ru(tpy)(bpy)Cl]Cl, [Ru(tpy)(pic)Cl], $[Ru(tpy)(tmen)Cl](PF_6)$, [Ru(tpy)(acac)Cl], and $[Ru(tpy)(ox)(H_2O)]$ were synthesized following literature procedures.[25,26] The ruthenium starting material ($RuCl_3 \cdot xH_2O$), silver trifluoromethanesulfonate (AgOTf), and silver hexafluorophosphate ($AgPF_6$) were purchased from Strem. The ligands, 2,2′:6′,2″-terpyridine (tpy), 2,2′-bipyridine (bpy), *N*,*N*,*N*′,*N*′-tetramethylethylenediamine (tmen), picolinic acid (Hpic), 2,4-pentanedione (Hacac), sodium malonate (Na_2mal), sodium oxalate (Na_2ox), and dimethyl sulfoxide (dmso) were purchased from Aldrich. Tetrabutylammonium hexafluorophosphate ($TBAPF_6$) was purchased from Fluka and recrystallized from hot ethanol three times. Acetonitrile and dichloromethane for electrochemical experiments were of spectroscopic grade and purchased from Burdick and Jackson. All other reactants and solvents were used without further purification.

[Ru(tpy)(pic)(dmso)](OTf). Dark purple [Ru(tpy)(pic)Cl] (218.4 mg, 0.428 mmol) was dissolved in 250 mL of 1,2-dichloroethane in the presence of excess dmso (500 μL) and 1 equiv (110.4 mg, 0.429 mmol) of AgOTf. The reaction mixture was refluxed under argon overnight. The reaction mixture turned from purple to a dark yellow during this time. The solution was filtered hot to remove 1 equiv of solid AgCl. The filtrate volume was reduced to 3−4 mL, and the yellow-orange product precipitated with the addition of ethanol. The product was isolated by vacuum filtration, washed with ethanol (2 × 15 mL) and ether (3 × 20 mL), and air-dried. Yield: 131.7 mg (45%). UV−vis (dmso) λ_{max} = 421 (5347 M^{-1} cm^{-1}). Emission (77 K) λ_{em} = 587, 667 nm. $E^{\circ\prime}$ $Ru^{3+/2+}$ vs Ag/AgCl = 1.38 V (S-bonded), 0.63 V (O-bonded). ^{1}H NMR (dmso-d_6): δ 9.78 (d, pic), 8.79 (d, tpy), 8.73 (d, tpy), 8.38 (t, pic), 8.23 (t, tpy), 8.04 (t, tpy), 7.92 (d, pic), 7.63 (t, tpy), 2.42 (s, dmso). ν(SO) = 1089 cm^{-1}.

[Ru(tpy)(bpy)(dmso)](OTf)$_2$. Red-brown [Ru(tpy)(bpy)Cl]Cl (279.4 mg, 0.49 mmol) was dissolved in 50 mL of 1,2-dichloroethane in the presence of excess dmso (1 mL) and 2 equiv (253.8 mg) of AgOTf. The reaction mixture was refluxed under argon for 4 h. The solution was filtered hot to remove 2 equiv of AgCl. The filtrate volume was reduced to 3−4 mL, and the yellow-orange product precipitated with the addition of ethanol. The product was isolated by vacuum filtration, washed with ethanol (2 × 15 mL) and ether (3 × 20 mL), and air-dried. Yield: 355.8 mg (85%). UV−vis (dmso) λ_{max} = 419 nm (8080 M^{-1} cm^{-1}). Emission (77 K) λ_{em} = 575, 670 nm. $E^{\circ\prime}$ $Ru^{3+/2+}$ vs Ag/AgCl = 1.67 V (S-bonded), 1.10 V (O-bonded). ^{1}H NMR (dmso-d_6): δ 9.99 (d, bpy), 8.95 (d, tpy), 8.76 (d, tpy), 8.59 (t, bpy), 8.46 (t, bpy), 8.19 (t, tpy), 8.08 (t, tpy), 7.81 (d, bpy), 7.52 (t, tpy), 7.34 (t, bpy), 7.12 (d, bpy), 2.48 (s, dmso). ν(SO) = 1102 cm^{-1}.

[Ru(tpy)(tmen)(dmso)](PF$_6$)$_2$. Purple $[Ru(tpy)(tmen)Cl](PF_6)$ (197.8 mg, 0.314 mmol) was dissolved in 125 mL of 1,2-dichloroethane in the presence of excess dmso (1 mL) and 1 equiv of $AgPF_6$ (90.0 mg). The reaction mixture was heated at reflux under argon atmosphere for 2 h. The reaction mixture turned from deep purple to a dark yellow-orange, and AgCl precipitated with some product. The mixture was filtered hot and washed with a minimal amount of dmso. One equivalent of AgCl was recovered. The filtrate volume was reduced to 3−4 mL, and the yellow-orange product precipitated with the addition of ethanol. The product was

(11) Fomitchev, D. V.; Bagley, K. A.; Coppens, P. *J. Am. Chem. Soc.* **2000**, *122*, 532−533.
(12) Kovalevsky, A. Y.; Bagley, K. A.; Coppens, P. *J. Am. Chem. Soc.* **2002**, *124*, 9241−9284.
(13) Yeh, A.; Scott, N.; Taube, H. *Inorg. Chem.* **1982**, *21*, 2542−2545.
(14) Tomita, A.; Sano, M. *Inorg. Chem.* **1994**, *32*, 5825−5830.
(15) Sano, M.; Taube, H. *Inorg. Chem.* **1994**, *33*, 705−709.
(16) Sano, M. *Struct. Bonding* **2001**, *99*, 117−139.
(17) Tomita, A.; Sano, M. *Inorg. Chem.* **2000**, *39*, 200−205.
(18) Smith, M. K.; Gibson, J. A.; Young, C. G.; Broomhead, J. A.; Junk, P. C.; Keene, F. R. *Eur. J. Inorg. Chem.* **2000**, 1365−1370.
(19) Rack, J. J.; Winkler, J. R.; Gray, H. B. *J. Am. Chem. Soc.* **2001**, *123*, 2432−2433.
(20) Rack, J. J.; Mockus, N. V. *Inorg. Chem.* **2003**, *42*, 5792−5794.
(21) Sens, C.; Rodriguez, M.; Romero, I.; Llobet, A.; Parella, T.; Sullivan, B. P.; Benet-Buchholz, J. *Inorg. Chem.* **2003**, *42*, 2040−2048.
(22) Rack, J. J.; Rachford, A. A.; Shelker, A. M. *Inorg. Chem.* **2003**, *42*, 7357−7359.
(23) Collier, C. P.; Wong, E. W.; Belohradsky, M.; Raymo, F. M.; Stoddart, J. F.; Kuekas, P. J.; Williams, R. S.; Heath, J. R. *Science* **1999**, *285*, 391−394.
(24) Steuerman, D. W.; Tseng, H.-R.; Peters, A. J.; Flood, A. H.; Jeppesen, J. O.; Nielsen, K. A.; Stoddart, J. F.; Heath, J. R. *Angew. Chem., Int. Ed.* **2004**, *43*, 6486−6491.
(25) Sullivan, B. P.; Calvert, J. M.; Meyer, T. J. *Inorg. Chem.* **1980**, *19*, 1404−1407.
(26) Dovletoglou, A.; Adeyemi, S. A.; Meyer, T. J. *Inorg. Chem.* **1996**, *35*, 4120−4127.

isolated by vacuum filtration, washed with ethanol (2 × 15 mL) and ether (3 × 20 mL), and air-dried. Yield: 126.5 mg (50%). UV−vis (dmso) λ_{max} = 429 nm (8161 M^{-1} cm^{-1}). Emission (77 K) λ_{em} = 590, 666 nm. $E^{\circ\prime}$ $Ru^{3+/2+}$ vs Ag/AgCl = 1.65 V (S-bonded), 1.03 V (O-bonded). ν(SO) = 1066 cm^{-1}.

[Ru(tpy)(acac)(dmso)](PF$_6$). Purple [Ru(tpy)(acac)Cl] (65.3 mg, 0.139 mmol) was dissolved in 50 mL of 1,2-dichloroethane in the presence of excess dmso (1 mL), and 1 equiv (36.0 mg) of $AgPF_6$ was added to the mixture and dissolved. The reaction mixture was refluxed under argon for 4 h. The mixture was filtered hot to recover 1 equiv of AgCl. The filtrate volume was reduced to 3−4 mL, and the product precipitated with the addition of a 100 mL ethanol/hexanes mixture (2:1). The product was isolated as a dark maroon solid upon recrystallization. The final solid was vacuum filtered, washed with hexanes (3 × 20 mL), and air-dried. Yield: 52.8 mg (60%). UV−vis (dmso) λ_{max} = 468 nm (5318 M^{-1} cm^{-1}). Emission (77 K) λ_{em} = 591, 682 nm. $E^{\circ\prime}$ $Ru^{3+/2+}$ vs Ag/AgCl = 0.95 V (S-bonded). ^{1}H NMR (dmso-d_6): δ 8.65 (d, tpy), 8.38 (d, tpy), 8.2 (m, tpy), 7.74 (t, tpy), 5.40 (s, acac), 2.63 (s, dmso), 2.32 (s, acac), 1.46 (s, acac). ν(SO) = 1088 cm^{-1}.

[Ru(tpy)(mal)(dmso)]. [Ru(tpy)(mal)(H_2O)] was prepared by following the procedure for [Ru(tpy)(ox)(H_2O)]. Dark purple [Ru(tpy)(mal)(H_2O)] (188.9 mg, 0.42 mmol) was partially dissolved in 125 mL of 1,2-dichloroethane in the presence of excess dmso (350 μL). The purple reaction mixture was refluxed under argon overnight. The filtrate volume was reduced to 3−4 mL, and the product precipitated with the addition of 100 mL ethanol/hexanes mixture (2:1). The maroon solid was isolated by vacuum filtration, washed with ether (3 × 20 mL), and air-dried. Yield: 128.3 mg (60%). UV−vis (dmso) λ_{max}, = 502 nm (5134 M^{-1} cm^{-1}). Emission (77 K) λ_{em} = 670 nm. $E^{\circ\prime}$ $Ru^{3+/2+}$ vs Ag/AgCl = 0.82 V (S-bonded). ^{1}H NMR (dmso-d_6): δ 9.01 (d, tpy), 8.51 (d, tpy), 8.14 (t, tpy), 8.02 (t, tpy), 7.78, (t, tpy), 3.58 (s, mal), 2.59 (s, dmso). ν(SO) = 1083 cm^{-1}.

[Ru(tpy)(ox)(dmso)]. Deep purple [Ru(tpy)(ox)(H_2O)] (43.0 mg, 0.098 mmol) was partially dissolved in 125 mL of 1,2-dichloroethane in the presence of excess dmso (1 mL). The reaction mixture was refluxed under argon for 4 h. The filtrate volume was reduced to 3−4 mL, and the product precipitated with the addition of 100 mL ethanol/hexanes mixture (2:1). The maroon solid was isolated by vacuum filtration, washed with ether (3 × 20 mL), and air-dried. Yield: 15.8 mg (32%). UV−vis (dmso) λ_{max} = 485 nm (4396 M^{-1} cm^{-1}). Emission (77 K) λ_{em} = 593, 666 nm. $E^{\circ\prime}$ $Ru^{3+/2+}$ vs Ag/AgCl = 0.86 V (S-bonded). ^{1}H NMR (dmso-d_6): δ 8.64 (d, tpy), 8.44 (d, tpy), 8.20 (t, tpy), 8.12 (t, tpy), 7.78 (t, tpy), 2.63 (s, dmso). ν(SO) = 1084 cm^{-1}.

[Ru(tpy)(bpy)(dms)](OTf)$_2$. This complex was prepared by substituting dimethyl sulfide (dms) for dmso in the procedure for [Ru(tpy)(bpy)(dmso)](OTf)$_2$. The photochemical and electrochemical data match previously reported values. UV−vis (CH_3CN) λ_{max} = 454 nm. Emission (77 K) λ_{em} = 590, 666 nm. $E^{\circ\prime}$ $Ru^{3+/2+}$ vs Ag/AgCl = 1.39 V.

[Ru(tpy)(pic)(dms)](PF$_6$). This complex was prepared by substituting dms for dmso in the procedure for [Ru(tpy)(pic)(dmso)](PF$_6$). UV−vis (CH_3CN) λ_{max} = 483, 368 nm. Emission (77 K) λ_{em} = 666 nm. $E^{\circ\prime}$ $Ru^{3+/2+}$ vs Ag/AgCl = 1.03 V.

[Ru(tpy)(mal)(py)]. Purple Ru(tpy)(mal)(OH_2) (146.7 mg, 0.32 mmol) was dissolved in 1,2-dichloroethane (125 mL) in the presence of excess pyridine (0.5 mL, 6 mmol). The reaction mixture was refluxed under argon overnight. The solution was reduced in volume to 3−4 mL. The product was precipitated by the addition of a 100 mL ethanol/hexanes mixture (2:1). Yield: 147.1 mg (88%). UV−vis (dmso) λ_{max} = 540, 482, 363 nm. $E^{\circ\prime}$ $Ru^{3+/2+}$ vs Ag/AgCl = 0.84 V.

[Ru(tpy)(pic)(CH_3CN)](PF$_6$). Solid [Ru(tpy)(pic)Cl] was dissolved in acetonitrile, and 1 equiv of AgPF6 was added. The resulting mixture was refluxed under argon for 4 h. The reaction mixture was filtered to remove 1 equiv of AgCl. The filtrate was then reduced in volume to ~5 mL, and ethanol (5 mL) was added. The addition of hexanes precipitated the maroon product. Yield: 40%. UV−vis (CH_3CN) [λ_{max}, nm (ϵ, M^{-1} cm^{-1})] 497 (4716), 456 (4434), 355 (4820). $E^{\circ\prime}$ $Ru^{3+/2+}$ vs Ag/AgCl = 0.87 V.

Instrumentation. Cyclic voltammetry was performed on a CH Instruments CH1730A electrochemical analyzer. The working electrode was a glassy-carbon electrode (BAS). The counter and reference electrodes were Pt wire and Ag/AgCl, respectively. Electrochemical measurements were typically performed in CH_3CN or CH_2Cl_2 solutions containing 0.1 M $TBAPF_6$ electrolyte in a one-compartment cell. Electronic absorption spectra were collected on an Agilent 8453 spectrophotometer. Bulk photolysis experiments were conducted using a 75 W xenon-arc lamp (Oriel). Infrared spectra were obtained on a Shimadzu Advantage FTIR-8400 spectrometer with KBr pellets. Proton nuclear magnetic resonance (^{1}H NMR) spectra were collected on a 250 MHz Bruker AG spectrometer in deuterated dmso (dmso-d_6) or deuterated dichloromethane (CD_2Cl_2). Emission spectra were collected at 77 K in 4:1 ethanol/methanol on a PTI C-60 fluorimeter equipped with a Hamamatsu R928 PMT (185−900 nm).

Crystallography. Crystals suitable for structural determination were obtained by slow evaporation of saturated acetonitrile/dmso solutions. The structure of [Ru(tpy)(ox)(dmso)] was determined at Kent State University (C. C. Raymond) on a Bruker-AXS SMART-CCD single-crystal diffractometer. Data were integrated with software provided by Bruker-AXS (SAINT 6.22), from which the final unit cell parameters were derived. Cell refinement was completed using SHELXL-97 (Sheldrick, 1997). Structures of [Ru(tpy)(pic)(dmso)](OTf), [Ru(tpy)(tmen)(dmso)](PF$_6$)$_2$, [Ru(tpy)(acac)(dmso)](PF$_6$), and [Ru(tpy)(mal)(dmso)] were determined at West Virginia University (J. L. Petersen). Single crystals were washed with the perfluoropolyether PFO-XR75 (Lancaster) and sealed under nitrogen in a glass capillary. Samples were optically aligned on the four-circle of a Siemens P4 diffractometer equipped with a graphite monochromatic crystal, a Mo Kα radiation source (λ = 0.71073 Å), and a SMART CCD detector. All crystal structures were drawn using ORTEP.

Quantum Yield of Isomerization. Quantum yields of isomerization were obtained by irradiating degassed solutions of [Ru(tpy)(L2)(dmso)]$^{z+}$ in *N*,*N*-butylmethylpyrrolidinium sulfonamide at 298 K.[27] Photolysis was achieved using a Continuum Nd:YAG laser pumped OPO (optical parametric oscillator) operating at 10 Hz. Incident radiation intensities were monitored by potassium ferrioxalate actinometry.

$$\phi tI = C_T V[\ln(C_T) - \ln(C_T - C_p)] \quad (1)$$

The procedure is similar to that originally described by McMillin for photosubstitution quantum yields in [Ru(tpy)(bpy)(CH_3CN)]$^{2+}$.[28−31] The irradiation wavelength corresponded to the

(27) MacFarlane, D. R.; Meaken, P.; Sun, J.; Amini, N.; Forsyth, M. *J. Phys. Chem. B* **1999**, *103*, 4164−4170.
(28) Kirchhoff, J. R.; McMillin, D. R.; Marnot, P. A.; Sauvage, J.-P. *J. Am. Chem. Soc.* **1985**, *107*, 1138−1141.
(29) Suen, H.-F.; Wilson, S. W.; Pomerantz, M.; Walsh, J. L. *Inorg. Chem.* **1989**, *28*, 786−791.
(30) Hecker, C. R.; Fanwick, P. E.; McMillin, D. R. *Inorg. Chem.* **1991**, *30*, 659−666.

lowest energy isosbestic point between S-bonded and O-bonded isomers. The integrated rate equation for determining

$$I = I_o(1 - 10^{-\epsilon C_T l}) \quad (2)$$

the quantum yield (ϕ) when irradiating at an isosbestic point is given in eq 1. Here, C_T and C_p are the total $[Ru(tpy)(L2)(dmso)]^{z+}$ concentration and the concentration of the photoproduct (O-bonded

$$\phi = \frac{C_T V[\ln(C_T) - \ln(C_T - C_p)]}{tI_o(1 - 10^{-\epsilon C_T l})} \quad (3)$$

dmso complex), respectively, V is the total volume of the solution (3 mL), t is the irradiation time, and I is the radiation intensity absorbed by the sample at the irradiation wavelength. The radiation intensity (I) at the cuvette face is determined by eq 2, where I_o is the incident radiation intensity, ϵ is the extinction coefficient, and l is the radiation path length. The incident radiation intensity is determined by ferrioxalate actinometry. Substitution of eq 2 into eq 1 yields eq 3, which is employed to calculate the isomerization quantum yield ($\phi_{S\rightarrow O}$). The concentration of the O-bonded isomer (C_p) was determined by monitoring the absorbance at a wavelength unique to this isomer.

Results

Synthesis. The complexes presented here were prepared using modifications to traditional synthetic routes. Reaction of $RuCl_3$ with terpyridine yields $Ru(tpy)Cl_3$ in good yield. This material is well-suited to the sequential addition of a bidentate ligand and a monodentate ligand to give the desired complex.[26] Refluxing the chloro starting materials ($[Ru(tpy)(L2)Cl]^z$, z dependent upon L2 charge) in dichloromethane or dichloroethane and small volumes of dmso (1 mL) yields the target dmso complexes in moderate yield. The complexes were recrystallized from dmso/acetonitrile solutions in the dark. With the exception of $[Ru(tpy)(pic)(dmso)]^+$, these complexes are readily manipulated in normal room light without concern for isomerization. However, exposure of $[Ru(tpy)(pic)(dmso)]^+$ to room light for extended periods does yield the O-bonded isomer. In solution, this is problematic since the O-bonded isomer is rapidly substituted by Lewis basic solvents (e.g., CH_3CN, EtOH).

Molecular Structures. The structures of *trans*-$[Ru(tpy)(pic)(dmso)]^+$ (pic is 2-picolinate) and $[Ru(tpy)(tmen)(dmso)]^{2+}$ (tmen is tetramethylethylenediamine) are shown in Figures 1 and 2. A summary of the crystallographic data is found in Table 1. These structures are similar to that of $[Ru(tpy)(bpy)(dmso)]^{2+}$ (bpy 2,2′-bipyridine).[19] In Figure 1, the pic structure shows the carboxylate oxygen trans to the dmso ligand, as predicted by absorption and electrochemical data (see below). The atoms of the first coordination sphere form a distorted octahedron and the terpyridine ligand features a puckering typical in these complexes. The metal−ligand bond distances are within the accepted tolerances for Ru−N and Ru−O bonds (Table 2). The dmso ligand in these structures is S-bonded; the Ru−S bond distance decreases from 2.2506(8) (tmen) to 2.2152(5) Å (pic), while the S−O

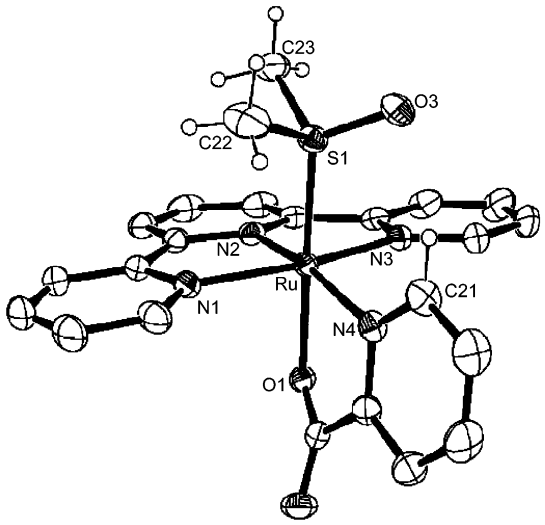

Figure 1. Molecular structure of $[Ru(tpy)(pic)(dmso)]^+$.

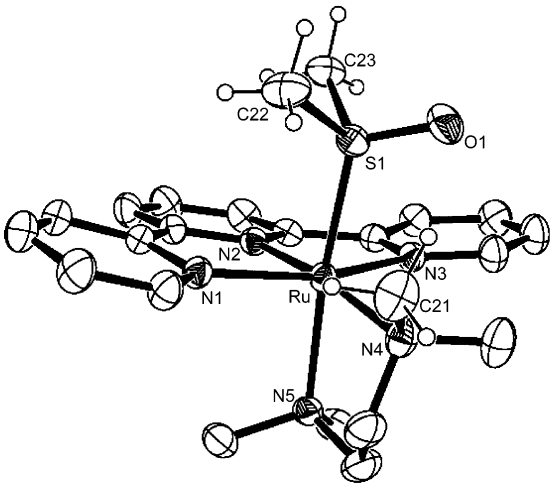

Figure 2. Molecular structure of $[Ru(tpy)(tmen)(dmso)]^{2+}$.

bond distances increase from 1.471(2) (tmen) to 1.479(2) Å (pic). The corresponding Ru−S and S−O bond distances for the bpy complex are 2.282(1) and 1.467(3) Å, respectively. The oxygen atom of dmso in these three structures is projected toward the bidentate ligand. The $O_{dmso}\cdots H-C_{L2}$ distance is ~3.0 Å, suggesting this O atom is likely involved in intramolecular H-bonding.[32−34]

The structures of $[Ru(tpy)(acac)(dmso)]^+$ (acac is acetylacetonate), $[Ru(tpy)(mal)(dmso)]$ (mal is malonate) and $[Ru(tpy)(ox)(dmso)]$ (ox is oxalate) are shown in Figures 3, 4, and 5, respectively. Again, the characteristic puckering of the terpyridine ligand is observed, and the Ru−N and Ru−O bond distances are within the accepted ranges (Table 3). The Ru−S bond distance continues to decrease from 2.2242(4) (acac) to 2.2203(5) (mal) to 2.206(2) Å (ox), while the S−O bond distance increases from 1.480(2) (acac) to 1.479(2) (mal) to 1.492(4) Å (ox) within this series. It is important to note that the Ru−S bond for the acac complex is not

(31) Bonnet, S.; Collin, J.-P.; Sauvage, J.-P.; Schofield, E. *Inorg. Chem.* **2004**, *43*, 8346−8354.

(32) Desiraju, G. R. *Acc. Chem. Res.* **1991**, *24*, 290−296.

(33) Reddy, P. A. N.; Nethaji, M.; Chakravarty, A. R. *Inorg. Chem. Commun.* **2003**, *6*, 698−701.

(34) Rodriguez-Martin, Y.; Lorenzo-Luis, P. A.; Gili, P.; Ruiz-Perez, C. *J. Coord. Chem.* **2003**, *56*, 181−191.

Table 1. Summary of Crystallographic Data for $[Ru(tpy)(L2)(dmso)]^{z+}$

L2 =	pic	tmen	acac	mal	ox
formula	$C_{24}H_{21}F_3N_4O_6RuS_2$	$C_{23}H_{33}F_{12}N_5OP_2RuS$	$C_{24}H_{30}F_6N_3O_4PRuS_2$	$C_{20}H_{24}N_3O_{7.5}RuS$	$C_{19}H_{17}N_3O_7RuS$
fw	683.64	818.61	734.67	559.55	532.49
T, K	295(2)	295(2)	295(2)	295(2)	568(2)
space group	$P2_1/c$	$P2_1/c$	$P\bar{1}$	$C2/c$	$P2_1/c$
a, Å	12.8400(8)	19.8629(11)	9.2333(5)	25.9361(16)	11.589(6)
b, Å	8.6442(5)	10.0815(5)	13.1204(8)	8.7363(6)	8.894(4)
c, Å	23.8890(15)	16.1698(9)	13.6893(8)	20.6139(13)	20.509(10)
α	90°	90°	69.540(1)°	90°	90°
β	93.957(1)°	104.651(1)°	73.733(1)°	107.902(1)°	101.832(10)°
γ	90°	90°	80.341(1)°	90°	90°
V, Å^3	2645.2(3)	3132.7(3)	1487.06(15)	4444.7(5)	2069.1
Z	4	4	2	8	4
ρ_{calc}, g/cm^{-3}	1.717	1.736	1.641	1.672	1.709
total reflns	18 022	21 540	10 567	13 597	12 400
inddependent reflns	5965	7145	6616	4943	2938
params	417	412	364	314	282
R1 (%)	3.51	4.14	4.15	3.78	3.86
wR2 (%)	8.23	10.61	11.26	10.74	10.65

Table 2. Selected Bond Distances and Angles for L2 = bpy, pic, and tmen

L2	distance	(Å)	angles	(deg)
bpy	Ru−N1	2.079(3)	N1−Ru−N3	158.7(1)
	Ru−N2	1.975(3)	N1−Ru−N2	79.4(1)
	Ru−N3	2.073(3)	N2−Ru−N3	79.5(1)
	Ru−N4	2.100(3)	N1−Ru−S	93.24(8)
	Ru−N5	2.084(3)	N2−Ru−S	91.30(8)
	Ru−S	2.282(1)	N3−Ru−S	90.31(8)
	S−O1	1.467(3)	N4−Ru−S	96.89(9)
	S−C26	1.779(5)	N5−Ru−S	174.03(9)
	S−C27	1.781(6)	O1−S−Ru−N4	42.55
pic	Ru−N1	2.076(2)	N1−Ru−N3	159.06(6)
	Ru−N2	1.959(2)	N1−Ru−N2	79.30(7)
	Ru−N3	2.069(2)	N2−Ru−N3	79.91(6)
	Ru−N4	2.101(2)	N1−Ru−S	94.96(5)
	Ru−O1	2.085(1)	N2−Ru−S	95.94(4)
	Ru−S	2.2152(5)	N3−Ru−S	89.66(4)
	S−O3	1.479(2)	N4−Ru−S	97.44(5)
	S−C22	1.769(3)	O1−Ru−S	176.05(4)
	S−C23	1.783(2)	O3−S−Ru−N4	51.7
tmen	Ru−N1	2.137(2)	N1−Ru−N3	156.52(9)
	Ru−N2	1.982(2)	N1−Ru−N2	78.79(9)
	Ru−N3	2.149(2)	N2−Ru−N3	78.12(9)
	Ru−N4	2.238(2)	N1−Ru−S	91.88(7)
	Ru−N5	2.228(2)	N2−Ru−S	92.90(7)
	Ru−S	2.251(1)	N3−Ru−S	85.15(7)
	S−O1	1.471(2)	N4−Ru−S	93.77(7)
	S−C22	1.785(4)	N5−Ru−S	174.23(7)
	S−C23	1.782(3)	O1−S−Ru−N4	44.7

statistically distinct from that of the pic complex. However, these data confirm the π-acid nature of S-bonded dmso in these complexes.[35−37] The trend of decreasing Ru−S bond distance is consistent with substitution of a π-acidic ligand (bpy) with a π donor (ox). The oxygen atom of dmso in these three complexes is projected over the terpyridine ligand. The $C-H_{dmso}\cdots O_{L2}$ distance is ∼3.0 Å, which is also suggestive of intramolecular hydrogen bonding.

Electrochemistry. Cyclic voltammagrams of $[Ru(tpy)(pic)(dmso)]^+$ and $[Ru(tpy)(tmen)(dmso)]^{2+}$ are qualitatively similar to those observed for $[Ru(tpy)(bpy)(dmso)]^{2+}$ and other ruthenium−dmso complexes which isomerize.[16] All three complexes feature voltammagrams whose appearance

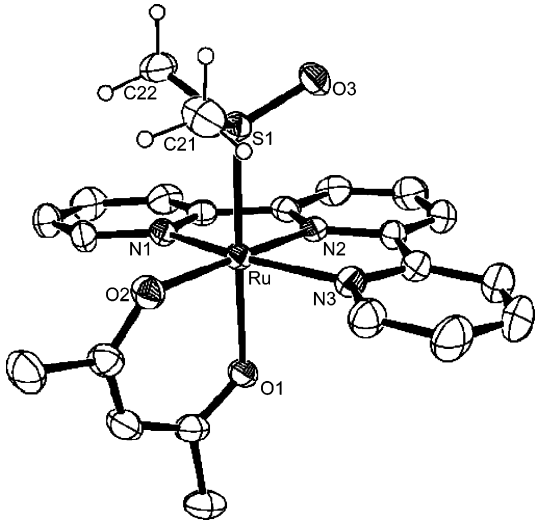

Figure 3. Molecular structure of $[Ru(tpy)(acac)(dmso)]^+$.

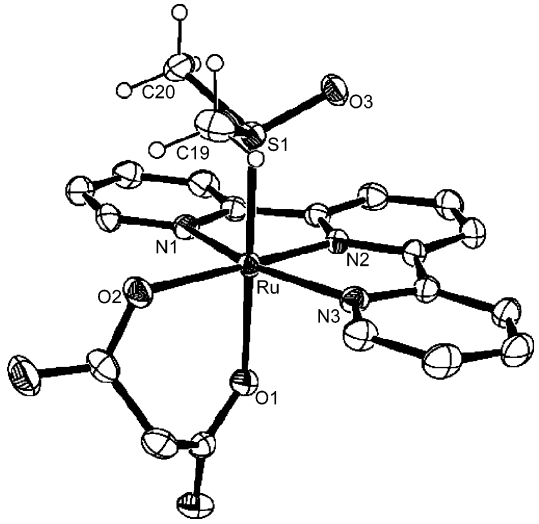

Figure 4. Molecular structure of $[Ru(tpy)(mal)(dmso)]$.

is dependent upon the scan rate. Shown in Figure 6 are cyclic voltammagrams of $[Ru(tpy)(pic)(dmso)]^+$. Two well-separated irreversible couples are observed at a scan rate of 0.1 V s^{-1}. Increasing the scan rate to ≥5 V s^{-1} shows the appearance of the cathodic wave for the couple at ∼1.4 V.

(35) Calligaris, M.; Carugo, O. *Coord. Chem. Rev.* **1996**, *153*, 83−154.
(36) Calligaris, M. *Coord. Chem. Rev.* **2004**, *248*, 351−375.
(37) Alessio, E. *Chem. Rev.* **2004**, *104*, 4203−4242.

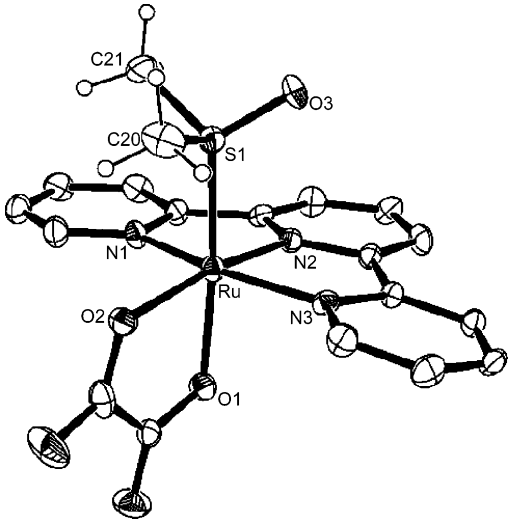

Figure 5. Molecular structure of [Ru(tpy)(ox)(dmso)].

Table 3. Selected Bond Distances and Angles for L2 = acac, mal, and ox

L2	distance	(Å)	angles	(deg)
acac	Ru−N1	2.062(1)	N1−Ru−N3	159.33(7)
	Ru−N2	1.942(2)	N1−Ru−N2	79.91(6)
	Ru−N3	2.080(2)	N2−Ru−N3	79.93(6)
	Ru−O1	2.072(1)	N1−Ru−S	93.57(4)
	Ru−O2	2.083(2)	N2−Ru−S	91.68(4)
	Ru−S	2.2242(4)	N3−Ru−S	91.50(4)
	S−O3	1.480(2)	O1−Ru−S	178.54(4)
	S−C21	1.782(2)	O2−Ru−S	90.21(4)
	S−C22	1.770(2)	O3−S−Ru−O1	149.0
mal	Ru−N1	2.054(2)	N1−Ru−N3	160.01(6)
	Ru−N2	1.951(2)	N1−Ru−N2	80.76(7)
	Ru−N3	2.103(2)	N2−Ru−N3	79.31(7)
	Ru−O1	2.111(1)	N1−Ru−S	91.52(4)
	Ru−O2	2.115(1)	N2−Ru−S	91.63(5)
	Ru−S	2.2203(5)	N3−Ru−S	90.57(4)
	S−O3	1.479(2)	O1−Ru−S	179.04(4)
	S−C19	1.780(2)	O2−Ru−S	90.60(4)
	S−C20	1.786(2)	O3−S−Ru−O1	159.7
ox	Ru−N1	2.056(5)	N1−Ru−N3	159.6(2)
	Ru−N2	1.951(5)	N1−Ru−N2	80.4(2)
	Ru−N3	2.072(5)	N2−Ru−N3	79.6(2)
	Ru−O1	2.090(5)	N1−Ru−S	92.9(2)
	Ru−O2	2.102(5)	N2−Ru−S	94.7(2)
	Ru−S	2.206(2)	N3−Ru−S	92.9(2)
	S−O3	1.492(4)	O1−Ru−S	173.9(1)
	S−C20	1.777(7)	O2−Ru−S	94.6(2)
	S−C21	1.793(7)	O3−S−Ru−O1	139.5

The most positive couple corresponds to $E^{\circ\prime}$ for the S-bonded isomer (Table 4). Scans which do not oxidize the S-bonded starting material do not reveal the low-energy couple (~0.7 V), indicating that this species is only formed following oxidation at higher potentials. The lower-energy couple is thus assigned to the O-bonded isomer, in accord with previous investigations.[13,18,19] The voltammagram is consistent with an ECEC mechanism in which S-to-O isomerization follows Ru(II) oxidation and O-to-S isomerization follows Ru(III) reduction.[38]

Simulations of the voltammagrams as a function of scan rate are consistent with this mechanism. Scheme 1 was used to analyze the electrochemical data. Due to our instrumental limitations, we are unable to accurately estimate an S-to-O isomerization rate (k_1) following Ru(II) oxidation directly from the voltammagrams. However, our evaluation of the O-to-S isomerization rate following Ru(III) reduction is in good agreement with independent bulk photolysis measurements (see below). The simulations suggest that the S-to-O rate (k_1) is >50 s^{-1} and the O-to-S rate is on the order of 10^{-3} s^{-1} for the complexes in this study.

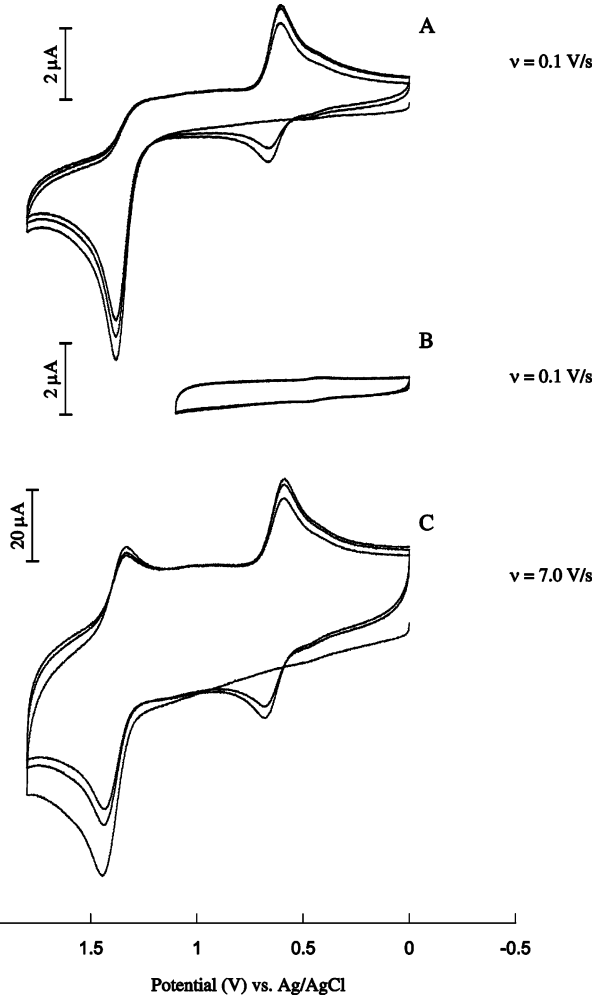

Figure 6. Cyclic voltammograms for $[Ru(tpy)(pic)(dmso)]^+$. (A) Voltammagram recorded at $\nu = 0.1$ V s^{-1}. (B) Voltammagram recorded at $\nu = 0.1$ V s^{-1}. Potential limits are 0 to +1.1 V, illustrating that a low-energy couple is formed only from oxidation at ~+1.5 V. (C) Voltammagram recorded at $\nu = 7.0$ V s^{-1}, illustrating quasi-reversible behavior for both high and low couples.

Voltammagrams of $[Ru(tpy)(acac)(dmso)]^+$ and [Ru(tpy)(mal)(dmso)] show reversible one-electron behavior over a wide range of scan rates (10−5 mV s^{-1}). Indeed, plots of I_p (peak current) vs $\nu^{1/2}$ are linear, and the ratio of I_{pa}:I_{pc} is one (see Supporting Information). These data indicate that these couples are reversible and that S-to-O isomerization does not occur following oxidation of Ru(II) at the electrode. This result does not appear to be dependent upon solvent or electrode material. The voltammagram of the oxalate complex is problematic. Our results are consistent with oxalate decomposition following Ru(II) oxidation. This complicated our electrochemical studies and prompted our investigation of the malonate complex.

(38) Nicholson, R. S.; Shain, I. *Anal. Chem.* **1964**, *36*, 706−723.

Table 4. Electrochemical and Photochemical Results for $[Ru(tpy)(L2)(dmso)]^{z+}$

L2	$E°'$ (S-bonded) (V)	$E°'$ (O-bonded) (V)	λ_{max} (S-bonded), nm (ϵ, M^{-1} cm^{-1})	λ_{max} (O-bonded), nm (ϵ, M^{-1} cm^{-1})	k_2 (O-to-S) (s^{-1})	$\phi_{S\rightarrow O}$
bpy	1.67	1.10	419 (8080)	490 (13668)	$1.4(3) \times 10^{-3}$	0.024(1)
pic	1.38	0.63	421 (5347)	527 (4524)	$1.0(3) \times 10^{-3}$	0.25(1)
tmen	1.65	1.03	429 (8161)	530 (7480)	$1.8(5) \times 10^{-3}$	0.007(1)
acac	0.95		468 (5318)			<0.0001
ox	0.86		485 (4396)			
mal	0.82		502 (5134)			

Scheme 1. Electrochemical Square Scheme for Observed Linkage Isomerization

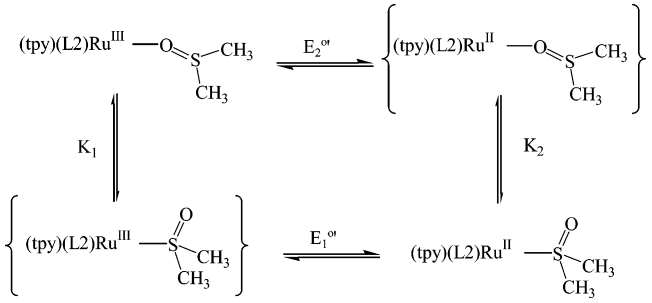

Photochemistry. Absorption maxima and intensities are shown in Table 4. Typical of ruthenium−polypyridine complexes, the spectra reveal low-energy visible charge-transfer transitions and ligand-centered transitions in the UV. Consistent with the structural and electrochemical data, the lowest-energy Ru dπ → tpy π* metal-to-ligand charge-transfer (MLCT) transition shifts to lower energy as the bipyridine ligand is replaced with less π-stabilizing ligands (Figure 7). This trend is consistent with destabilization of the t_{2g} dπ orbital set following substitution of the π-acid (bipyridine) ligand with a π-base ligand (oxalate or malonate). The absorption maxima are indicative of S-bonded dmso, as evidenced by the blue shift of the lowest-energy MLCT transition relative to the corresponding chloro or aquo starting materials.

The complexes containing bpy, tmen, pic, and acac exhibit phototriggered isomerization in solution, in ionic liquid (*N*,*N*-butylmethylpyrrolidinium sulfonimide), and in the solid state. Shown in Figure 8 are representative data of the linkage isomers of the pic complex in ionic liquid. Irradiation into the MLCT band of the S-bonded isomer produces the O-bonded isomer, which absorbs at lower energy. Direct measurement of the S → O rate is too rapid for our instrumentation. However, the appearance of the same O-bonded product in differing low-donor organic solvents (halogenated solvents, propylene carbonate) and ionic liquid suggests that this reaction occurs intramolecularly.[19,20,22] Irradiation of these complexes in high-donor solvents (pyridine, CH_3CN) ultimately yields the solvent adducts, which are formed following isomerization. Similar to the S-bonded absorption maxima, the O-bonded absorption maxima follow the expected trend with changes in the ligand field strength of the bidentate ligand (Figure 9).

Photoisomerization quantum yields (Table 4) were determined in ionic liquid for the complexes that display isomerization. The bpy ($\phi_{S\rightarrow O} = 0.024 \pm 1$) and pic ($\phi_{S\rightarrow O} = 0.25 \pm 1$) complexes feature much greater quantum yields of isomerization than the tmen ($\phi_{S\rightarrow O} = 0.007 \pm 1$) and acac ($\phi_{S\rightarrow O} < 0.0001$) complexes. Continued irradiation of the malonate sample did not reveal evidence for isomerization. These quantum yields are greater than those obtained for

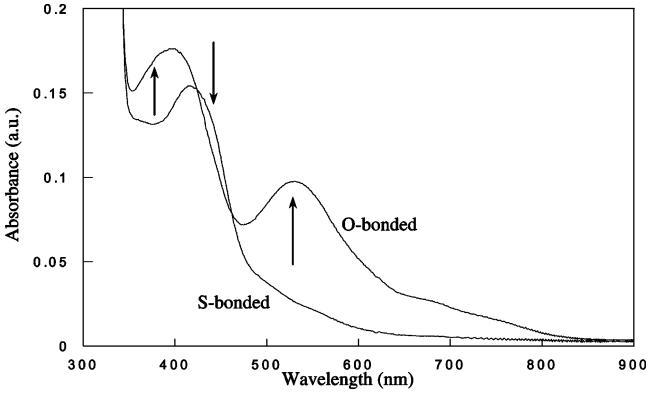

Figure 8. Absorption Spectra of S- and O-bonded $[Ru(tpy)(pic)(dmso)]^+$ in ionic liquid.

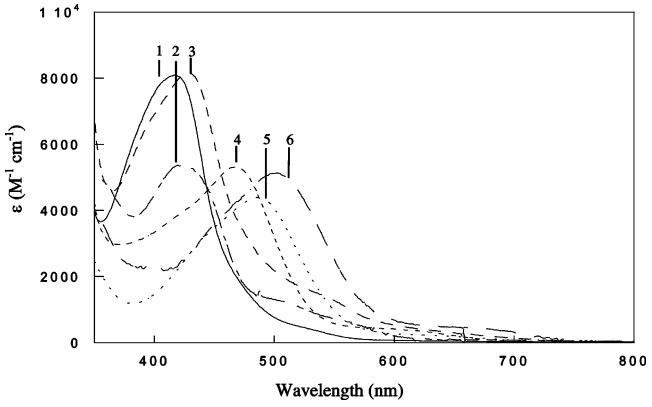

Figure 7. Absorption spectra of S-bonded $[Ru(tpy)(L2)(dmso)]^{z+}$ complexes in dmso. 1, L2 = bpy; 2, L2 = pic; 3, L2 = tmen; 4, L2 = acac; 5, L2 = ox; 6, L2 = mal.

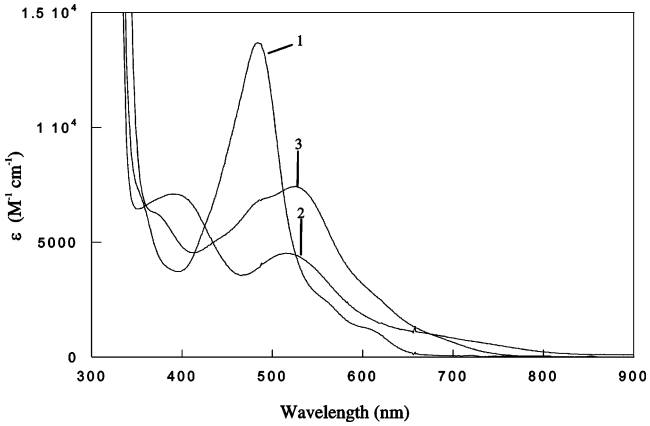

Figure 9. Absorption spectra of O-bonded complexes in dmso. 1, L2 = bpy; 2, L2 = pic; and 3, L2 = tmen.

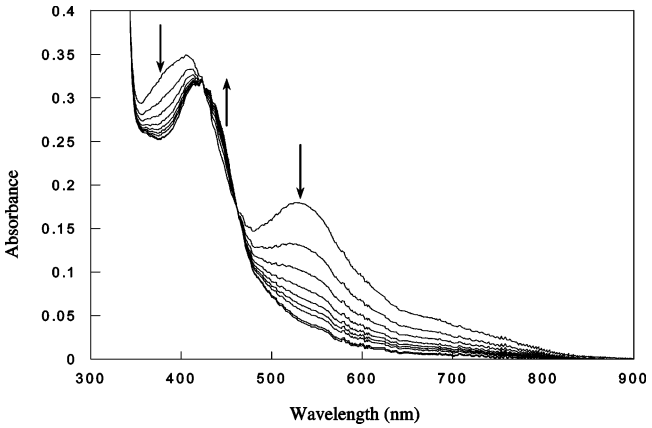

Figure 10. Reversion of O-bonded $[Ru(tpy)(pic)(dmso)]^+$ in ionic liquid.

photosubstitution reactions of ruthenium polypyridine chemistry, indicating that isomerization occurs by a different mechanism than photosubstitution. In our procedure, we irradiate ionic liquid solutions containing the dmso complexes at the longer-wavelength isosbestic point. The procedure accounts for the changing concentration of the reactant. The quantum yields vary by more than 3 orders of magnitude on the basis of the identity of the bidentate ligand.

For the complexes that do feature S-to-O isomerization, thermal reversion to the S-bonded isomer from the O-bonded isomer is observed in certain organic solvents, ionic liquids, and the solid state. Shown in Figure 10 are representative data of the pic complex in ionic liquid. Reaction rates vary from 1.8×10^{-3} to 1.0×10^{-3} s^{-1} for the three complexes (Table 4), and the isosbestic point suggests direct formation of the S-bonded isomer from the O-bonded isomer without an intervening intermediate. A first-order plot (Supporting Information) verifies the intramolecular nature of this reaction. The rates of isomerization appear to be solvent independent as they are similar in dmso and halogenated solvents.

Discussion

Synthesis. While Meyer reports formation of both cis and trans isomers of [Ru(tpy)(pic)(Cl)] from $Ru(tpy)Cl_3$, our procedure yields the trans isomer exclusively.[26] This isomer features the picolinate oxygen trans to the sulfoxide. Column chromatography of the chloro material does not reveal isolable *cis*-[Ru(tpy)(pic)(Cl)] and did not improve the yield during the dmso ligand-substitution reaction. There is no evidence for isomerism of the pic ligand (cis−trans) during reflux of this complex in halogenated solvent. Thin-layer chromatography did not show the presence of *cis*-$[Ru(tpy)(pic)(dmso)]^+$.

Molecular Structures. The structural data for the family of $[Ru(tpy)(L2)(dmso)]^{z+}$ complexes shows that the Ru−S bond distance decreases from 2.282(1) (bpy) to 2.206(2) Å (ox), while the S−O bond distance increases from 1.467(3) to 1.492(4) Å. Such a trend is consistent with the notion that dmso is acting as a π acid. However, the S−O bond distance in uncomplexed, free dmso is 1.521(5) Å, indicating that the S−O distance is shorter, and the bond is stronger, in these structures than it is in free dmso.[39] One expects the bonded S−O distance to be longer in these complexes than in unbound dmso if dmso is acting as a π acid. Further inspection of the structure does not reveal a favorable bonding interaction between a ruthenium dπ orbital and a dmso π^* orbital. A comparison of the dihedral angle defined by N4−Ru−S1−O_{dmso} shows that this angle is 51.7° and 44.7° for the pic and tmen complexes, respectively (Table 2). This angle in the bpy complex is 42.6°. For the acac, ox, and mal complexes, the corresponding angle involving the O−S−Ru (dmso) and O−Ru−S (L2) planes is 149°, 139.5°, and 159.7°, respectively (Table 3). Essentially, this angle represents rotation of dmso about the Ru−S bond. A large angle is not expected to favor a traditional π back-bonding interaction between ruthenium and π^* orbital of dmso. A pyramidal geometry about the sulfur atom also disfavors this interaction. In agreement with the structural data, IR spectra of these complexes consistently reveal that ν(SO) > 1055 cm^{-1}, the value obtained for free, uncomplexed dmso.[35] Bonding involving the S−C σ^* orbitals is unlikely, as these distances are essentially invariant for the complexes discussed here. The distances span 1.779(5) and 1.781(6) Å for the bipyridine complex to 1.780(2) and 1.786(2) Å for the malonate complex. These asymmetric S−C distances are in accord with those observed for free dmso (1.766(8) and 1.827(11) Å).[39] Thus, despite the compelling trend in the Ru−S and S−O bond lengths, an argument for π back-bonding involving the sulfoxide π^* orbital is difficult to visualize. The observed large dihedral angle in the dmso structures is the result of maximizing σ dmso donation with e_g^* set and back-donation from the t_{2g} set with the π^* orbital of dmso. The π interaction is likely to be similar to that observed in metal phosphine complexes.[40,41]

A similar conclusion was reported by Schugar in his evaluation of $(NH_3)_5Ru^{II}$−thioether bonding.[42] In this report, he noted that, while structural and spectroscopic evidence strongly support the notion of Ru(II)−dms back-bonding, computational or theoretical verification of this assignment was not identified. Not unlike Ru−dmso bonding, large tilt (Ru−S−R) and twisting (dihedral) angles about the Ru−S bond were observed in this study. This geometry is expected to minimize steric interactions and maximize bonding between Ru (x^2-y^2, xy) and S (s, pπ) lone pairs in Ru−thioether bonding.[42] A similar bonding interaction is likely operative in these dmso structures.

The puckering that is often observed in terpyridine structures is evident in these complexes.[43−45] Except for the tmen complex, the terpyridine ligand is puckered or bent away from the dmso ligand. The short, strong Ru−S interaction does not appear to ruffle the terpyridine ligand.

(39) Thomas, R.; Shoemaker, C. B.; Eriks, K. *Acta Crystallogr.* **1966**, *21*, 12−20.
(40) Orpen, G. A.; Connelly, N. G. *Organometallics* **1990**, *9*, 1206−1210.
(41) Xiao, S.-X.; Trogler, W. C.; Ellis, D. E.; Berkovitch-Yellin, Z. *J. Am. Chem. Soc.* **1983**, *105*, 7033−7037.
(42) Krogh-Jespersen, K.; Zhang, X.; Ding, Y.; Westbrook, J. D.; Potenza, J. A.; Schugar, H. J. *J. Am. Chem. Soc.* **1992**, *114*, 4345−4353.
(43) Rasmussen, S. C.; Ronco, S. E.; Mlsna, D. A.; Billadeau, M. A.; Pennington, W. T.; Kolis, J. W.; Petersen, J. D. *Inorg. Chem.* **1995**, *34*, 821−829.

Recently determined structures of $[Ru(tpy)(phen)(L)]^{2+}$ (phen is 1,10-phenanthroline; L is CH_3CN, py, or phenothiazine) show similar distortions.[45] The phenothiazine structure is notable in that the Ru−S bond distance is 2.375(3) Å, which is ∼0.01 Å longer than the longest Ru−S bond distance discussed here, and yet it features a ruffling typical of terpyridine. For $[Ru(tpy)(tmen)(dmso)]^{2+}$, the terpyridine ligand is puckered toward the dmso ligand. One interpretation for this change is that the steric demands of the methyl groups on tmen are greater than that of dmso. Coincidentally, the structure of $[Ru(tpy)(tmen)(OH_2)]^{2+}$ displays a similar distortion, indicating that the methyl groups of tmen are likely responsible for this structural change.[46]

The orientation of the dmso ligand and the relatively short C−H···O distances are suggestive of intramolecular hydrogen bonding.[32] For L2 = bpy, tmen, and pic, the S−O bond of the dmso ligand is oriented toward a C−H bond of the bidentate ligand. The O···C separations associated with the corresponding hydrogen-bonding interactions for the bpy, pic, and tmen complexes are 3.117 (O1···C16), 3.272 (O1···C21), and 3.407 Å (O1···C18), respectively. While the distance in the tmen complex is long, these distances are within the acceptable ranges for intramolecular C−H···O hydrogen bonds in coordination complexes.

For the complexes containing O-donor, π-basic ligands, the S−O bond is projected over the terpyridine ligand away from the bidentate ligand. In these cases, a C−H bond of a methyl group from dmso appears hydrogen bonded to the coordinated bidentate ligand. The O···C separations associated with the corresponding hydrogen-bonding interactions involving acac, mal, and ox are 3.019 (O1···C21), 3.137 (O1···C20), and 3.041 Å (O1···C20), respectively, again within the expected ranges for hydrogen bonding. On the basis of these structural data, it is reasonable to suggest that the bidentate ligand plays a role in determining the orientation of the dmso ligand.

Electrochemistry. A shift to lower energy in $E^{\circ\prime}$ is observed for S-bonded $[Ru(tpy)(L2)(dmso)]^{2+}$ as L2 is varied from a π acid (bpy) to a π base (mal, ox). The range in $E^{\circ\prime}$ is from 1.67 (vs Ag/AgCl) for $[Ru(tpy)(bpy)(dmso)]^{2+}$ to 0.82 V (vs Ag/AgCl) for [Ru(tpy)(mal)(dmso)] and spans more than 800 mV. A similar trend, but smaller in magnitude, is seen for the corresponding aquo complexes.[26] In those cases, $E^{\circ\prime}$ = 0.49 V (vs SCE) for $[Ru(tpy)(bpy)(OH_2)]^{2+}$ which cathodically shifts to $E^{\circ\prime}$ = 0.19 and 0.16 V (vs SCE) for $[Ru(tpy)(acac)(OH_2)]^{+}$ and $[Ru(tpy)(ox)(OH_2)]$, respectively. The comparison between aquo and dmso complexes illustrates the π-stabilization of the Ru t_{2g} set by dmso relative to water. A π-acidic ligand environment is expected to yield a large, positive reduction potential (pic, 1.38 V vs Ag/AgCl), whereas the presence of a π base is anticipated to stabilize the higher oxidation state and shift $E^{\circ\prime}$ to lower energy (mal, 0.82 V vs Ag/AgCl).

When L2 is bpy, tmen, or pic, these complexes feature electron-transfer-triggered linkage isomerization (Figure 6). These three complexes all exhibit an anodic wave at large, positive potential, while the corresponding cathodic wave is not apparent at slow scan rates (<1 V s^{-1}). A new couple appears at lower potential at the expense of the higher-energy couple. A comparison of current densities of each wave demonstrates the four states illustrated in Scheme 1 adequately describe the voltammagram. At large scan rates (>5 V s^{-1}), a cathodic wave for the high-energy couple is observed and the current passed at the low-energy couple is correspondingly smaller.

The appearance of the voltammagram is a consequence of the ratio of the scan rate and isomerization rate. Simulations of the voltammagrams provide a procedure for determining reaction rate constants following electron transfer. Our best estimates from simulations based on Scheme 1 suggest that $k_{S\rightarrow O} > 50\ s^{-1}$. Observance of the cathodic peak of the high-potential couple requires fast scan rates (>10 V s^{-1}) which generates much nonfaradaic current resulting in a poor voltammagram. Our evaluation of $k_{O\rightarrow S}$ from the simulation is more reliable ($\sim 10^{-3}\ s^{-1}$) as it can be independently measured from bulk photolysis (see below).

Reversible electrochemistry is observed for the complexes containing acac or mal over a large range of scan rates (10−1 mV s^{-1}). The peak separation in the S-bonded Ru(III/II) couple suggests little molecular movement following oxidation and reduction. For the acac and mal complexes, $\Delta E_{pk} = E_{p,a} - E_{p,c}$ = 0.067 and 0.066 V, respectively. For comparison, we prepared $[Ru(tpy)(bpy)(dms)]^{2+}$ and $[Ru(tpy)(pic)(dms)]^{+}$ and determined ΔE_{pk} = 0.066 V ($E^{\circ\prime}$ = 1.39 V) and ΔE_{pk} = 0.066 V ($E^{\circ\prime}$ = 1.03 V), respectively. The peak separation for [Ru(tpy)(mal)(py)] (py is pyridine) is 0.080 V ($E^{\circ\prime}$ = 0.84 V). Thus, while the peak potential separation for $[Ru(tpy)(acac)(dmso)]^{+}$ and [Ru(tpy)(mal)(dmso)] is larger than that described by the Nernst equation, it is not unreasonable for complexes of this type.

It is not immediately obvious why the Ru−dmso complexes containing acac and mal do not support the formation of their respective O-bonded isomers following Ru(II) oxidation. In terms of Hard−Soft Acid−Base theory, this observation suggests that the Ru(III) in these complexes is not "hard" enough to promote the S-to-O isomerization. This explanation does not suggest whether the O-bonded surface is thermodynamically unfavorable or kinetically inaccessible. It is reasonable to conclude that the S-bonded and O-bonded surfaces are affected differently during the substitution of the bidentate ligand in this family of complexes.

Sulfoxide isomerizations in $[Ru(NH_3)_5]^{3+/2+}$ fragments have been investigated by Taube, Sano, and co-workers.[13−17] They demonstrated that rates of S → O isomerization on Ru(III) may be increased by roughly $10^4\ s^{-1}$ by substituting *s*-butyl for methyl on the sulfoxide ligand.[14,16] In contrast, the O → S isomerization rate was invariant to these changes. For $[Ru(NH_3)_5(dmso)]^{3+/2+}$, they found $k_{S\rightarrow O}$ = 0.37 s^{-1} (ΔG^* = 74 kJ mol^{-1}) on Ru^{3+} and $k_{O\rightarrow S}$ = 14 s^{-1} (ΔG^* = 66 kJ mol^{-1}) on Ru^{2+}.[13] Comparison of these studies by Sano with our results and setting $k_{S\rightarrow O} = 50\ s^{-1}$ as a lower limit

(44) Gerli, A.; Reedijk, J.; Lakin, M. T.; Spek, A. L. *Inorg. Chem.* **1995**, *34*, 1836−1843.
(45) Bonnet, S.; Collin, J.-P.; Gruber, N.; Sauvage, J.-P.; Schofield, E. *J. Chem. Soc., Dalton Trans.* **2003**, 4654−4662.
(46) Grover, N.; Gupta, N.; Singh, P.; Thorp, H. H. *Inorg. Chem.* **1992**, *31*, 2014−2020.

suggests that the activation barrier for S → O isomerization (ΔG^*) is smaller on Ru^{3+} and that the O → S activation barrier is larger on Ru^{2+} ($k_{O\rightarrow S} \approx 10^{-3}$ s^{-1}) in the $[Ru(tpy)(L2)(dmso)]^{3+/2+}$ complex. There must be a substantial change in the electronic structure of these complexes when the O-donor bidentate ligands are incorporated within the complex. This appears to be the only set of complexes in which the triggering of dmso isomerization has been deactivated.

Photochemistry. For the complexes with bpy, pic, or tmen, the MLCT absorption maxima are shifted to an energy not typically seen for ruthenium polypyridine complexes.[47] For example, the absorption maximum of $[Ru(bpy)_3]^{2+}$ is 452 nm, which shifts to 348 nm for $[Ru(bpy)_2(dmso)_2]^{2+}$, demonstrating the greater stabilizing ability of the dπ orbital set by dmso relative to bpy.[18,20] Similarly, the charge-transfer absorption maxima of the pic (421 nm) and the tmen (429 nm) complexes are shifted to higher energy relative to $[Ru(bpy)_3]^{2+}$. The spectral blue-shift is consistent with the positively shifted Ru(III/II) reduction potentials. The absorption maxima of the $[Ru(tpy)(L2)(dmso)]^{z+}$ complexes containing acac (468 nm), mal (502 nm), or ox (485 nm) do not readily display the effect of the dmso ligand. Instead, the π-basic ligands shift the MLCT absorption maxima to much lower energies. These maxima are consistent with mixed-ligand complexes containing strong- and weak-field ligands. For example, $[Ru(tpy)(acac)(H_2O)]^+$ and $[Ru(tpy)(H_2O)_3]^{2+}$ feature absorption maxima at 542 and 544 nm, respectively.[48]

Visible irradiation of solutions and microcrystalline powders of $[Ru(tpy)(bpy)(dmso)]^{2+}$, $[Ru(tpy)(pic)(dmso)]^{2+}$, and $[Ru(tpy)(tmen)(dmso)]^{2+}$ result in drastic changes in the visible absorption spectrum. As shown in Table 4, for the complexes which isomerize, the new low-energy absorption feature is consistent with O-bonded dmso. These low-energy absorption maxima are similar to those observed for the corresponding aquo complexes. For example, the absorption maxima for $[Ru(tpy)(bpy)(OH_2)]^{2+}$, $[Ru(tpy)(pic)(OH_2)]^+$, and $[Ru(tpy)(tmen)(OH_2)]^{2+}$ are 477, 491, and 520 nm, respectively, which compare well with the absorption maxima for O-bonded $[Ru(tpy)(bpy)(dmso)]^{2+}$ (490 nm), $[Ru(tpy)(pic)(dmso)]^+$ (527 nm), and $[Ru(tpy)(tmen)(dmso)]^{2+}$ (530 nm).

Thermal reversion of the metastable O-bonded isomer to the S-bonded starting material occurs for the $[Ru(tpy)(bpy)(dmso)]^{2+}$, $[Ru(tpy)(pic)(dmso)]^+$, and $[Ru(tpy)(tmen)(dmso)]^{2+}$ complexes. Despite the changes in the S-bonded and O-bonded reduction potentials ($\Delta E^{o\prime} = \Delta E_S{}^{o\prime} - \Delta E_O{}^{o\prime}$), there appears to be little change in $k_{O\rightarrow S}$ (Table 4). For the bpy, pic, and tmen complexes, $\Delta E^{o\prime}$ is 0.57, 0.75, and 0.62 V, respectively, and corresponds to a driving force of 13.1, 17.3, and 14.3 kcal, respectively. This rate does not appear to have a linear dependence on the driving force, suggesting that the activation barrier for O-to-S isomerization has shifted in response to the new driving force. Apparently, the differences in the bidentate ligand are great enough to prevent the observation of a linear free-energy relationship.

The quantum yields for isomerization ($\phi_{S\rightarrow O}$) are listed in Table 4 and increase in the order of L2 = acac (<0.0001), tmen (0.007), bpy (0.024), and pic (0.25). The quantum yield for photosubstitution of CH_3CN in $[Ru(tpy)(bpy)(NCCH_3)]^{2+}$ by pyridine in acetonitrile solution is 0.0016(2), which agrees well with the literature value of 0.0013(1) initially reported by McMillin and later by Collin.[28,30,31] These authors agree that photosubstitution proceeds by a dissociative mechanism involving a reactive ^{3}d−d or ligand field (^{3}LF) state, which is thermally accessible from the lowest energy ^{3}CT (charge transfer) state. While it would be convenient, it does not appear that intervention of the LF states during isomerization is required to explain our data.

As the bidentate ligand is replaced with weaker-field ligands, the e_g* set is stabilized or lowered until they are near in energy with the CT state. This is the typical argument to explain weak CT emission from certain ruthenium−polypyridine complexes.[49] Lowering of the LF states leads to more efficient crossing from the CT state to the LF state, which results in weak emission. The isomerization quantum yield data support this basic mechanism with smaller isomerization yields for $[Ru(tpy)(tmen)(dmso)]^{2+}$and $[Ru(tpy)(acac)(dmso)]^+$ than for $[Ru(tpy)(bpy)(dmso)]^{2+}$ and $[Ru(tpy)(pic)(dmso)]^+$. However, the order of magnitude increase in $\phi_{S\rightarrow O}$ of $[Ru(tpy)(pic)(dmso)]^+$ relative to $[Ru(tpy)(bpy)(dmso)]^{2+}$ suggests more than just the LF is changing. In contrast to the isomerization quantum yield, it is interesting to note that the photosubstitution quantum yield for $[Ru(tpy)(pic)(NCCH_3)]^+$ ($\phi = 0.0042$) only increases slightly relative to the bpy complex ($\phi = 0.0016$). If isomerization and photosubstitution occurred by a similar mechanism, then isomerization and photosubstitution quantum yields would be expected to be similar for $[Ru(tpy)(pic)(dmso)]^+$ and $[Ru(tpy)(bpy)(dmso)]^{2+}$. These data suggest that a LF mechanism is not operative in the excited-state isomerization of dmso.

Reference to photoisomerization and photosubstitution data of relevant osmium complexes is required at this point. In contrast to $[Ru(tpy)(bpy)(NCCH_3)]^{2+}$, $[Os(tpy)(bpy)(NCCH_3)]^{2+}$ does not undergo photosubstitution with pyridine in acetonitrile solutions, presumably due to the inaccessibility of the ^{3}LF states.[30] If ^{3}LF states are involved in isomerization, then the larger ligand field energy gap should prohibit isomerization. However, $[Os(bpy)_2(dmso)_2]^{2+}$ exhibits S → O photoisomerization ($\phi_{S\rightarrow O} = 0.042(1)$) and room-temperature emission ($\phi_{EM} = 0.21(2)$) in acetonitrile solution, signifying that photosubstitution and photoisomerization do not occur by similar mechanisms.[50]

The difference in the donor atom trans to dmso in the $[Ru(tpy)(pic)(dmso)]^+$ and $[Ru(tpy)(bpy)(dmso)]^{2+}$ complexes are responsible for the differences in $\phi_{S\rightarrow O}$. On the basis of π-bonding arguments, the pic ligand would stabilize the S-bonded dmso to a greater extent than the bpy ligand. In

(47) Juris, A.; Balzani, V.; Barigelletti, F.; Campagna, S.; Belser, P.; Von Zelewsky, A. *Coord. Chem. Rev.* **1988**, *84*, 88−277.
(48) Adeyemi, S. A.; Dovletoglou, A.; Guadalupe, A. R.; Meyer, T. J. *Inorg. Chem.* **1992**, *31*, 1375−1383.
(49) Kober, E. M.; Meyer, T. J. *Inorg. Chem.* **1984**, *23*, 3877−3886.
(50) Mockus, N. V.; Rack, J. J. unpublished results, 2005.

the former case, a π donor is opposite that of a π-stabilizing ligand, while in the latter two π-stabilizing ligands are trans to one another. On the basis of this approach, a stronger Ru−S bond (pic) might result in a smaller $\phi_{S\rightarrow O}$. In contrast, the data support the notion that π-donation from the picolinate oxygen into the Ru(III) MLCT excited-state weakens the Ru−S bond eventually leading to bond breaking and isomerization. The excited state would feature a shorter $Ru-O_{pic}$ bond than in the ground state. In the excited state, the compressed Ru−O bond labilizes the Ru−S bond, leading to isomerization. While the same action is operative in the bpy analogue, the amount of compression of the Ru−N bond trans to the sulfoxide is expected to be much smaller. The exact details of this interaction are speculative but remain the focus of future studies.

Isomerization Mechanism. It is interesting to note that the three complexes that isomerize all have the S−O bond directed toward the bidentate ligand, whereas the complexes that do not isomerize have the S−O projected over the terpyridine ligand. It is not immediately clear what role this orientation may have on the isomerization. One may envision a twisting or rotation about the Ru−S bond which results in a repulsive interaction between the bidentate ligand and the dmso ligand. Specifically, steric crowding would be experienced between a methyl group of dmso and H21 of bpy, pic, and tmen during this rotation. This interaction would result in a distortion of the bidentate ligand or a lengthening of the Ru−S bond. A lengthening of this bond would favor bond breaking and isomerization. In the structures with L2 = acac, ox, or mal, a lengthening of the Ru−S is not expected for this rotation. Full rotation about the Ru−S bond is unhindered by the presence of these ligands. It is tempting to suggest that a critical geometry element for isomerization requires rotation about the Ru−S bond.

Ligand rotations bound to ruthenium have recently been studied by Drew et al. in $[Ru(bpy)_2Cl]^+$ phosphonite (e.g., P(OH)(OEt)(Ph) and $P(OEt)_2(Ph)$ where Ph is phenyl) complexes.[51,52] In these complexes, rotation about the Ru−P bond is affected through irradiation ($\lambda > 460$ nm). The atropisomers or rotational isomers are monitored by CD (circular dichroism) spectroscopy, where the Ph group interacts with a pyridine ring of bipyridine to produce a measurable CD signature. Reminiscent of the hydrogen bonding between dmso and the bidentate ligand described above, hydrogen bonding between the phosphonite and bipyridine ligands is observed. Importantly, this rotation has no effect on the visible portion of the spectrum where charge-transfer bands are typically located. There are two major implications from this study relevant to dmso isomerization. First, this indicates that the substantial changes in the electronic spectrum are not due to a simple rotation of the dmso ligand. Second, this study implies that rotation of phosphonite, and by analogy, dmso occurs following charge-transfer excitation. These studies support the argument that dmso rotation is an important vibration in the photoisomerization mechanism.

The progression of events leading to excited-state dmso isomerization involves the formation of a thermally relaxed ^{3}MLCT state following charge-transfer excitation. It is reasonable to suggest that this occur on a sub-picosecond time scale as ^{3}MLCT formation in $[Ru(bpy)_3]^{2+}$ is complete in 300 fs.[53,54] The ligand-localized excited-state features a weakened Ru−S bond due to an absence of π-bonding between Ru and S. The excited-state dmso orientation is unlike that of the ground-state geometry, with twisting, bending, and lengthening of the $Ru-S_{dmso}$ bond possible distortions. Further rotation of the sulfoxide increases steric repulsion with the neighboring C−H bond of the bidentate ligand, causing isomerization over a relatively low energy barrier.[19] Crossing this threshold leads to formation of the lower-energy O-bonded Ru−dmso excited state, which relaxes nonradiatively to a ground-state O-bonded dmso surface. The ^{3}LF state is also thermally accessible from the initial S-bonded ^{3}MLCT state though higher in energy than the O-bonded manifold. Crossing this barrier leads to nonradiative decay to form an S-bonded ground state and is similar to excited-state deactivation in $[Ru(bpy)_3]^{2+}$. Those complexes that do not isomerize have a ^{3}MLCT state which is more strongly coupled to a ^{3}LF state and an O-bonded manifold that is less accessible.

Conclusion

Our investigations indicate that dmso isomerization in ruthenium must occur within a strong-field ligand environment. Isomerization in these complexes occurs following formation of an equilibrated S-bonded excited state. In these cases, the ^{3}LF states are higher in energy than the S → O activation barrier. Following isomerization, nonradiative decay produces the O-bonded metastable state, which yields the S-bonded state on a much longer time scale (k_2) along the ground-state energy surface. Introduction of weaker-field ligands into the complex lowers the ^{3}LF states, favoring a nonradiative transition to an S-bonded ground state. These low-lying excited states prevent movement into the O-bonded manifold. Future studies will continue to focus on the electronic and steric factors important for isomerization.

Acknowledgment. The authors thank P. Greg van Patten and Hugh H. Richardson for helpful discussions and Nicholas V. Mockus for experimental assistance. This work is supported in part by ACS PRF (38071-G3) and the Condensed Matter and Surface Sceinces (CMSS) program at Ohio University.

Supporting Information Available: CIF files for $[Ru(tpy)(L2)(dmso)]^{z+}$ structures, where L2 is pic, tmen, acac, ox, and mal; first-order plots of O-to-S isomerization. This material is available free of charge via the Internet at http://pubs.acs.org.

IC050778R

(51) Hesek, D.; Hembury, G. A.; Drew, M. G. B.; Taniguchi, S.; Inoue, Y. *J. Am. Chem. Soc.* **2000**, *122*, 10236−10237.
(52) Hesek, D.; Hembury, G. A.; Drew, M. G. B.; Borovkov, V. V.; Inoue, Y. *J. Am. Chem. Soc.* **2001**, *123*, 12232−12237.
(53) Damrauer, N. H.; Cerullo, G.; Yeh, A.; Boussie, T. R.; Shank, C. V.; McCusker, J. K. *Science* **1997**, *275*, 54−87.
(54) Yeh, A. T.; Shank, C. V.; McCusker, J. K. *Science* **2000**, *289*, 935−938.